

Finding a Replacement for Hexavalent Chromium Sacrificial Paint
Capstone Final Report

MSE 4592 - Materials Design Capstone II

The University of Virginia

In collaboration with Rolls-Royce Corporation and Luna Labs USA LLC

May 7th, 2025

Team Cr VI

Katie Anderson, Jesper Braley, Marcus Dupart

Contact Information

Collaborators:

Luna Labs, LLC:

Adam Goff (adam.goff@lunalabs.us)

Dr. Rebecca Marshall (rebecca.marshall@lunalabs.us)

Grace Le (grace.le@lunalabs.us)

Abhijai Marthur (abhijai.mathur@lunalabs.us)

Rolls-Royce Corporation:

Robert Golden (robert.golden@rolls-royce.com)

Brad Wiley (brad.wiley@rolls-royce.com)

UVA Mentorship:

Dr. James Fitz-Gerald, Capstone Advisor (jmf8h@virginia.edu)

Dr. Robert Kelly, Subject Matter Expert (rgk6y@virginia.edu)

Authors:

Katie Anderson (rpk8mj@virginia.edu)

Jesper Braley (exk9er@virginia.edu)

Marcus Dupart (phj6rt@virginia.edu)

Table of Contents

Capstone Preliminary Report.....	1
Contact Information.....	2
Table of Contents.....	3
Table of Figures.....	5
Executive Summary.....	7
Project Timeline.....	9
I. Fall 2024.....	9
II. Spring 2025.....	10
Cost Data and Constraints.....	11
Project Challenges.....	12
Coupon Test Plans.....	13
Experimental Procedures and Equipment Used.....	14
HTB Application and Curing.....	14
Thermal Screening and Isothermal Holds.....	15
Salt Fog Corrosion Testing.....	15
Results.....	16
Coating Adhesion and Blistering.....	17
Thermal Screening.....	22
Isothermal Holds.....	23
Salt Fog Testing.....	24
Discussion.....	31
Zinc Clad II Plus Overcoating.....	31
Degree of Rusting on Un-Scribed Coupons from Salt Fog.....	32

Rust Undercutting in Scribed Coupons from Salt Fog.....	32
Sol-Gel Barrier Coatings.....	33
Conclusions and Future Work	35
Acknowledgements.....	36
References.....	37
Further Reading	39
Appendix.....	40

Table of Figures

Table I. Hex-chrome health effects by body part. Toxic effects heavily depend on how hex-chrome enters the body. (ATSDR, 2023)	7
Figure 1. Schematic of Rolls Royce Trent 800 series engine with gold color in right schematic showing the steel shaft (Mustafa et al, 2024).	8
Figure 2. Spring 2025 testing timeline.....	10
Table II. Project budget.....	11
Table III. Scale and Description of Rust Ratings	13
Figure 3. Final substrate distribution.	14
Figure 4. Proposed alternative substrate distribution.....	14
Figure 5. CM Furnace 1218BL; Luna scribing device, clamped to table.....	16
Figure 6. Surface topography (a) of an unnamed Jotatemp IOZ coating (Jotun, n.d). Rolls Royce publication (b) showing cross section of IPcote 9183R1 coating (Wiley, 2022).	16
Figure 7. (a) Substrate appearance directly after sol-gel application (before sol-gel curing); (b) IPcote samples sent by RR.....	17
Table IV. ASTM D3359 crosshatch adhesion scale.	18
Figure 8. Scribe Adhesion testing (a) and ASTM D3359 (b) crosshatch adhesion testing of ZC base coat.....	18
Figure 9. ZC-only coupon surface view from (a) SEM at 1650x and (b) light microscope.	19
Figure 10. ASTM D3359 crosshatch adhesion test of HTB1 coating matrix.	19
Figure 11. ASTM D3359 crosshatch adhesion test of HTB2 coating matrix.	20
Figure 12. ASTM D3359 crosshatch adhesion test of HTB3 coating matrix.	20

Figure 13. (a) ASTM D3359 crosshatch adhesion test of HTB4 coating matrix and ASTM D714 (b) blistering scale.	21
Figure 14. HC coupon surface view from SEM at 1000x.....	21
Figure 15. ZC-only coating surface and adhesion testing after thermal cycling.	22
Figure 16. ZC+HTB3 thermal screening	23
Table V. Thermal screening results.	23
Figure 17. (a) ZC+HTB1 after 200°C hold and salt fog testing (Luna, 2025); (b) 150X Hirox micrograph showing red rust in scribe.....	24
Figure 18. (a) ZC+HTB2 after 300°C hold and salt fog testing (Luna, 2025); (b) 100X Hirox micrograph of HTB2 scribe.	25
Figure 19. (a) ZC+HTB3 after 400°C hold and salt fog testing (Luna, 2025); (b) 100X Hirox micrograph of HTB3 scribe.	26
Figure 20. (a) ZC+HTB4 after 300°C hold and salt fog testing (Luna, 2025); (b) 150X HTB4 Hirox micrograph.....	27
Figure 21. ASTM D610-08 for ZC Only. General rust count inside the boxes: 74.....	28
Figure 22. ASTM D610-08 for HTB3, from two different substrates. The average number of rust spots is 29.....	29
Figure 23. ASTM D610-08 for HTB4, from two different substrates. The average number of rust spots is 16.....	30

Executive Summary

The goal of this project was to find alternatives to an aluminum-based hex-chrome sacrificial paint matrix meant to protect the steel shaft of turbine engines (Figure 1). Viable replacements must have long-term corrosive and thermal resistance properties comparable to hex-chrome, survive at least 400°C, and be nontoxic.

Hexavalent chromium is the +6-oxidation state of chromium (Cr) and, like lead, is classified as a heavy metal. It is used in the production of stainless steel, stainless-steel production, electroplating, leather tanning, textile manufacturing, pigments, and wood preservation (NIEHS, 2024). First officially acknowledged as carcinogenic in the late 1900s, hex-chrome is able to bypass cell walls in the human body with ease (Shin et al., 2023). Of the health effects listed in Table I, perhaps the most insidious is the ability of hex-chrome to cause cancer that can lie dormant for 20 to 35 years (IARC, 1990).

Table I. Hex-chrome health effects by body part. Toxic effects heavily depend on how hex-chrome enters the body. (ATSDR, 2023)

<i>Contact Method</i>	<i>Effects</i>
General	DNA damage
Inhalation (dust from salt form)	Asthma Lung cancer; or non-cancerous, abnormal tissue growth in lungs Sinus irritation Pulmonary fibrosis
Touch (most often in industrial settings)	Chromate allergic dermatitis (dry skin, skin fissures, scaling, papules; Cr-protein formation via binding with skin cells) Erosive ulceration (holes in skin)
Ingestion (via contaminated groundwater, food, air; most often affects public health)	Blood toxicity Kidney disease Intestinal cancer Male infertility Gastrointestinal tract diseases Oxidative stress: cell, protein, DNA damage

The 1990 publication from the International Agency for Research on Cancer (IARC) marked one of the first well-known instances in which hex-chrome was acknowledged as a carcinogen (Birnbaum et al., 2021). In 2006, the U.S. Environmental Protection Agency (EPA) and Occupational Safety and Health Administration (OSHA) passed new hex-chrome regulations (Worthy & Belsky, 2006). Since 2017, the European Union has worked to phase out use of hex-chrome with REACH legislation (Wiley 2014). The Material Technology Center at Rolls Royce

has been tasked with getting rid of substances like hex-chrome in their material systems (Fitz-Gerald, 2024).

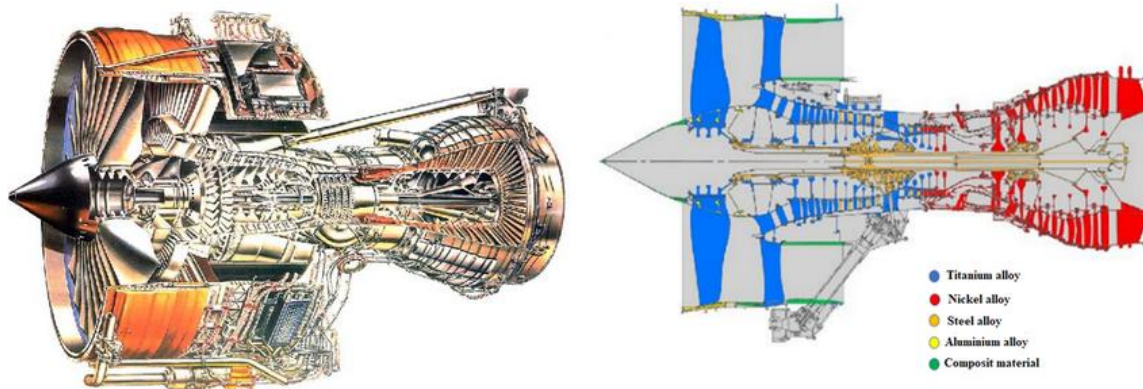


Figure 1. Schematic of Rolls Royce Trent 800 series engine with gold color in right schematic showing the steel shaft (Mustafa et al, 2024).

To accomplish this, the team created two-layer coating matrices from pre-existing commercial solutions and applied them to a low-carbon steel substrate. Sherwin Williams (SW) provided the team with 30 4" x 6" x 0.032" AISI 1010 steel Q-panel coupons coated in an 8mm thick layer of Zinc Clad II Plus. This Zinc Clad II Plus base coat has the same self-healing capabilities as hex-chrome, does not galvanically corrode the AISI 1010 substrate, and has functioned well with previous Luna coatings. Since the High Temperature Blockade (HTB) barrier coating by Luna Labs was in early development at the inception of the project, four different variations were tested on top of the SW Zinc Clad II Plus. HTB topcoats were about 5-7 μm thick.

The 30 substrates were split into five subgroups, each consisting of six coupons: Zinc Clade Plus (ZC) only, ZC and HTB1, ZC and HTB2, ZC and HTB3, ZC and HTB4. One substrate from each group underwent thermal screening. For each group, the official 24-hour isothermal hold temperatures were set to be 100 degrees below screening samples exhibited significant microcracking or adhesion loss.

After isothermal holds, the five official samples from each group entered the ASTM B117 salt fog chamber. Since the spring semester, the research portion of this capstone project, constrained the typical length of corrosion testing (ranging from one or two months to multiple years), three substrates within each subgroup were scribed to accelerate coating degradation. Additionally, the two hex-chrome containing substrates from Rolls Royce (RR) will allow for direct comparison of coating performance. They were coated with IPcote 9138R1 from

Indestructible Paint LLC. Of the two hex-chrome substrates, one was scribed. See Figure 3 for a diagram of the substrate coating plan.

After 12 days, one un-scribed and one scribed substrate were removed from the ASTM B117 salt fog testing chamber. All other coupons were left in the salt fog chamber for Luna to observe their behavior over a longer period. HTB3 performed the best in the thermal screening test, surviving up to 500°C. The following salt fog testing revealed the corrosion protection of HTB1 and HTB3 proved to be the best. Taking performance in thermal screening and salt fog into account, HTB3 has the most potential to be a hex-chrome replacement.

Project Timeline

I. Fall 2024.

Fall 2024 consisted of project selection and concept design. RR and Luna Labs (Luna) had each sent in two projects for consideration. September concluded with the class dividing into two teams based on their chosen projects; this team selected the hexavalent chromium sacrificial paint project from Rolls Royce. Immediately after project selection, design brainstorming began, culminating in the Conceptual Design Report finalized on October 10th. This report focused on background and initial concept generation. The report presented the impact of hex-chrome on environmental and human health, existing alternatives to chromium-based coatings, and concepts the team generated to solve the issue of hex-chrome.

In this first semester, the team considered creating a new coating, characterizing corrosion resistance of substrates processed in industry practices like bluing and metal cladding, and testing the popular trivalent chromium alternative. After discussing many less feasible ideas, the team was able to create three possible routes for the project: (1) designing a new testing environment or procedure to better evaluate new coatings, (2) testing existing alternative coating(s) to hexavalent chromium, and (3) combining existing coatings to screen new coating matrices. The third concept showed the most promise; a combination of coatings would provide more protection than any existing alternative would alone, especially since researchers have made no breakthroughs in over twenty years of research into hexavalent chromium alternatives. No existing coating matches the capabilities of hexavalent chromium.

From October 10th to November 1st, the team began to specify the plan for experimentation in the Preliminary Design Report which included: candidates for substrates and coatings, the application of these coatings, testing, and a timeline. The Detailed Design Report submitted on

November 25th mostly finalized substrate and coating selection. The substrate was to be AISI 1010, the base coat Zinc Clad II Plus by SW, and the topcoats variations of the HTB barrier coating in development at Luna Labs. At this point, the exact number of HTB variants was unknown. This first detailed design proposed ramping thermal exposure instead of separate, progressive isothermal holds. The team had also neglected to include many of the finer details, such as when substrates should be removed from salt fog chambers and imaged.

The team presented this first detailed design on December 3rd to the capstone class, subject matter experts (SMEs), and industry partners. SMEs and industry partners challenged the team to resolve the finer details in the experimental procedures. The primary feedback was (1) to specify that the purpose of this project is only for screening and (2) that isothermal holds work better than ramping for coatings in early development.

II. Spring 2025.

Testing Schedule	March	April			
	Week 4	Week 1	Week 2	Week 3	Week 4
Characterization of one uncoated, untested sample from each group					
Testing: Thermal					
Testing: ASTM B117 salt spray testing, conducted at Luna					
Characterization: Light microscopy (LM) imaging of samples					
Characterization: Scanning electron microscopy (SEM)					

Figure 2. Spring 2025 testing timeline

Physical experimentation and data analysis began in Spring 2025 (Figure 2). At the beginning of the semester, the team updated the Detailed Design Report to include more detailed testing procedures, resubmitting it on January 15th. On January 7th, the team had ordered 40 AISI 1010 substrates coated in Zinc Clad II Plus from SW—these samples took over one month and a half to arrive. The team also requested RR to send samples coated with the hex-chrome-based coating to form a control group; these two panels arrived on January 30th. After taking some basic macroscopic and optical microscopic images, the team gave both hex-chrome panels to the machinist to section for scanning electron microscope analysis on February 19th.

After a two-month wait and multiple emails and phone calls to SW, only 30 of the requested 40 Zinc Clad II Plus coupons arrived on February 27th. The team adjusted to this by redistributing sample groups. One Zinc Clad II coupon was left with the machinist to cut for scanning electron microscopy (SEM) analysis; the rest were delivered to Luna Labs on March 3rd to be coated with the four versions of HTB. The machinist returned sectioned substrates on March 5th, after which

basic optical microscope and macroscopic images were taken. On March 17th, SEM and Energy Dispersive Spectroscopy (EDS) analysis verified the Zinc Clad II coating composition. From March 8th to the 16th, spring break for UVA, Luna finalized HTB compositions and coated SW substrates. Thermal screening ran from March 25th to April 1st. 24-hour isothermal holds for the main substrates ran from April 1st to April 4th.

On April 7th, the team went to Luna to scribe and mask (tape) each substrate for salt fog testing. ASTM B117 salt fog testing only ran for a week and a half, from April 8th to April 18th. While this amount of time was adequate for the screening discussed in this report, observing the behavior of samples over a longer period is always better when it comes to salt fog testing. The team left two scribed and one un-scribed sample from each group with Luna for them to continue observation and development of their HTB coatings.

Cost Data and Constraints

Table II. Project budget

Item / action	Source	Cost per hour (\$)	Estimated time	Total (\$)
SW Q-panels coated with Zinc Clad II Plus	Sherwin Williams	-	-	Free
HVLP deposition of HTB coating variants onto SW Q-panels	Luna Labs	-	-	~1,000
Hexavalent chromium panels	Rolls-Royce	-	-	Free
Sample sectioning	Tanner	-	-	200
Scribing and taping	Luna, Capstone team			Free
Hirox imaging	Capstone team	17	5 hr	85
SEM imaging	Capstone team	17	~2 hr	34
Total				\$1,319

SW permits testing of its coatings, so Zinc Clad-coated AISI 1010 panels were free. The two hexavalent chromium panels from RR were also free, likely leftovers from a previous project.

The team will send Luna a purchase order which includes the time spent coating the SW substrates with the Blockade variants, which they estimate to be around \$1000.

With the added time it took for (1) SW panels to arrive and (2) Luna to narrow down chemistry for the four coating variants, testing was pushed to fit into the last week of March and the first three weeks of April. Moreover, samples were not able to survive at temperatures comparable to hexavalent chromium. In addition to SW sending 10 samples fewer than the requested amount, all substrates were also overcoated three to four times the amount needed for Zinc Clad II Plus.

Project Challenges

The team ran into countless challenges that affected the project design and, ultimately, the final data that could be collected. When ordering the coated substrates from SW, the team requested 40, which would have allowed for a redistribution of substrates into four different subgroups: ZC only, ZC and HTB1, ZC and HTB2, and ZC and HTB3. The ZC-only group would only have five substrates while the other three sub-groups would have ten each, with five extras remaining. A greater number of substrates could have allowed the team to also vary HTB thickness within each group, and the screening might have provided more information. Figure 4 shows this alternative testing plan. When only 30 coupons arrived, the plan in Figure 3 had to be developed.

At the beginning of March, the team discovered that Luna had since progressed in their own research, and Luna needed to finalize new formulations of Blockade to be screened. This pushed the timeline back an additional two weeks. After all testing, one week of thermal screening and ten days of salt fog testing, this cascade of mishaps pushed analysis time into the last week and a half of April. To prevent excess stress on future groups, the team recommends that all projects finish any testing at the end of March. Report finalization and characterization should occur in April. Ideally, final characterization should not overlap with final exams.

Another challenge that occurred during this project was a significant adhesion issue between the AISI 1010 steel substrate and the Zinc Clad II Plus base coat (Figure 5). Based on personal communication with Luna, this issue is one that they have also experienced. However, Luna noted that it has not decreased corrosion resistance in the past.

The final challenge that occurred during the project was the removal of coatings for red rust evaluation using ASTM D-1654-24. This standard involves the removal of the coating matrix around the scribe to observe potential rust creepage or undercutting. An example of how

this process should look can be seen in the Appendix. The mean creepage would then be established and a rating would be given from 10 to 0, with No.10 referring to no creepage and No.0 over 16mm to creepage (ASTM, 2024). However, due to the Zinc Clad II being chemically bonded to the low carbon substrate, it was impossible to remove the bond coat. This made it extremely difficult to determine the degree of red rust using this methodology. For that reason, the team switched to using ASTM 610–08 as the primary evaluation method, described in Table III. This standard involves visually inspecting the substrates to determine the type of rust distribution using preset definitions and estimating the surface area of rust (ASTM, 2019).

Table III. Scale and Description of Rust Ratings



Rust Grade	Percent of Surface Rusted	Visual Examples		
		Spot(s)	General (G)	Pinpoint (P)
10	Less than or equal to 0.01 percent		None	
9	Greater than 0.01 percent and up to 0.03 percent	9-S	9-G	9-P
8	Greater than 0.03 percent and up to 0.1 percent	8-S	8-G	8-P
7	Greater than 0.1 percent and up to 0.3 percent	7-S	7-G	7-P
6	Greater than 0.3 percent and up to 1.0 percent	6-S	6-G	6-P
5	Greater than 1.0 percent and up to 3.0 percent	5-S	5-G	5-P
4	Greater than 3.0 percent and up to 10.0 percent	4-S	4-G	4-P
3	Greater than 10.0 percent and up to 16.0 percent	3-S	3-G	3-P
2	Greater than 16.0 percent and up to 33.0 percent	2-S	2-G	2-P
1	Greater than 33.0 percent and up to 50.0 percent	1-S	1-G	1-P
0	Greater than 50 percent		None	

Rust Distribution Types:

S: Spot Rusting—Spot rusting occurs when the bulk of the rusting is concentrated in a few localized areas of the painted surface. The visual examples depicting this type of rusting are labeled 9-S through 1-S (See Fig. 1, Fig. 2, and Fig. 3).

G: General Rusting—General rusting occurs when various size rust spots are randomly distributed across the surface. The visual examples depicting this type of rusting are labeled 9-G through 1-G. (See Fig. 1, Fig. 2, and Fig. 3).

P: Pinpoint Rusting—Pinpoint rusting occurs when the rust is distributed across the surface as very small individual specks of rust. The visual examples depicting this type of rusting are labeled 9-P through 1-P. (See Fig. 1, Fig. 2, and Fig. 3).

H: Hybrid Rusting—An actual rusting surface may be a hybrid of the types of rust distribution depicted in the visual examples. In this case, report the total percent of rust to classify the surface. 9-H through 1-H.

Coupon Test Plans

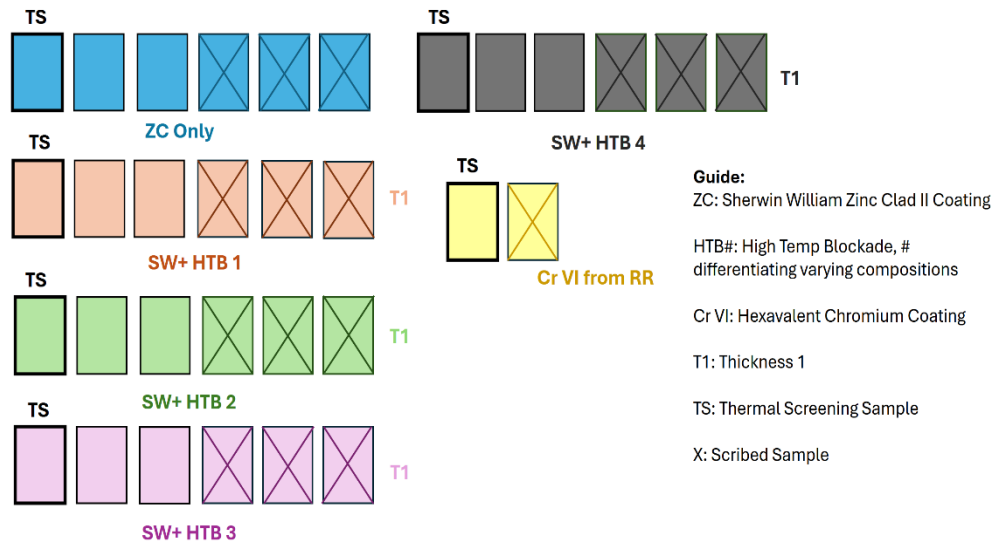


Figure 3. Final substrate distribution.

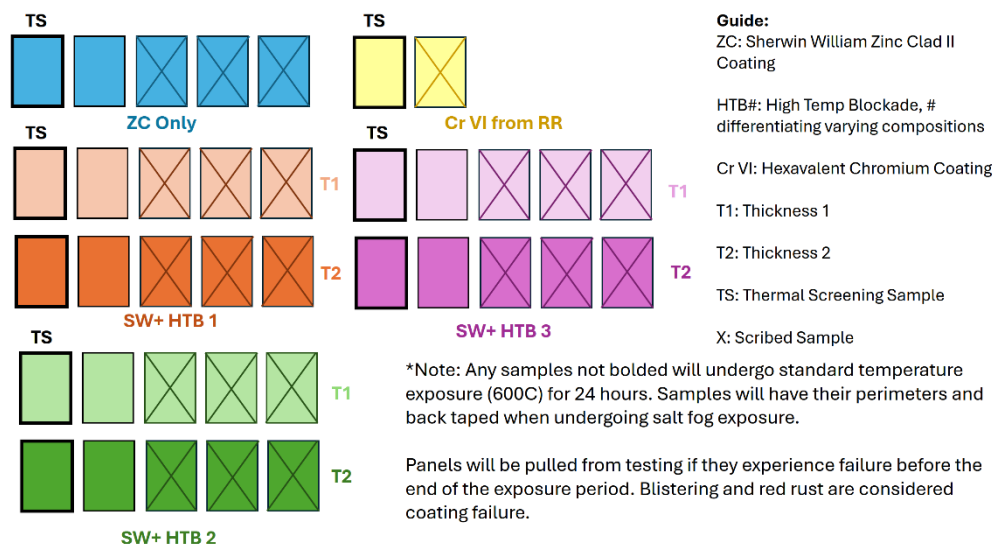


Figure 4. Proposed alternative substrate distribution.

Experimental Procedures and Equipment Used

HTB Application and Curing.

Luna applied HTB sol-gel coatings with high volume low pressure (HVLP) spray, a common, fast, and cost-effective way to coat substrates. The gun used was the DeVilbiss 802342 StartingLine Gravity Spray Gun with a 1 mm nozzle and a pressure of around 18.5 psi. After coating deposition, coupons were cured for three days at room temperature. HTB1 samples were

force-cured at 150°C for an additional hour, while HTB2, HTB3, and HTB4 samples were force-cured at 225°C for three hours.

Thermal Screening and Isothermal Holds.

After Luna coated all substrates with their designated HTB coating, one substrate from each subgroup was used in thermal screening. Isothermal holds began at 250°C, increasing to 300°C after a 21-hour exposure window. After 300°C, the temperature increased in 100-degree increments, stopping at 600°C. For thermal screening at 250°C and 300°C, the Binder FD23 oven was used. The CM Furnace 1218BL was used for temperatures 400°C and above. Between each hold in the furnace, substrates were cooled to room temperature. When they cooled, pencil hardness and ASTM D3359 crosshatch adhesion tests were conducted on the substrates. The samples would then be placed back in the furnace at the next highest temperature.

After thermal screening, the five main samples from each group were held for 24 hours at the temperature just below microcracking or adhesion loss began. From the thermal screening, the isothermal hold for ZC was 500°C; HTB1 at 200°C; HTB2 at 300°C; HTB3 at 400°C; and HTB4 at 300°C. The Binder FD23 oven held groups designated for 300°C and below, while the CM Furnace 1218BL held the groups at 400°C and above.

Salt Fog Corrosion Testing.

Following the isothermal holds, samples were scribed, taped, then placed within a Singleton SCCH23 chamber running the ASTM B117 procedure. A custom Luna device was used to scribe samples. The substrates were exposed to this environment from April 8th to April 18th, with images being taken every 24 hours. On the 18th, one scribed and one un-scribed substrate were removed from the chamber and examined optically using the Hirox RH-8800 Light Microscope for any signs of corrosion (red rust, etc.). Substrates were then sectioned and examined in the SEM, with EDS to examine corrosion products and other compositional information.

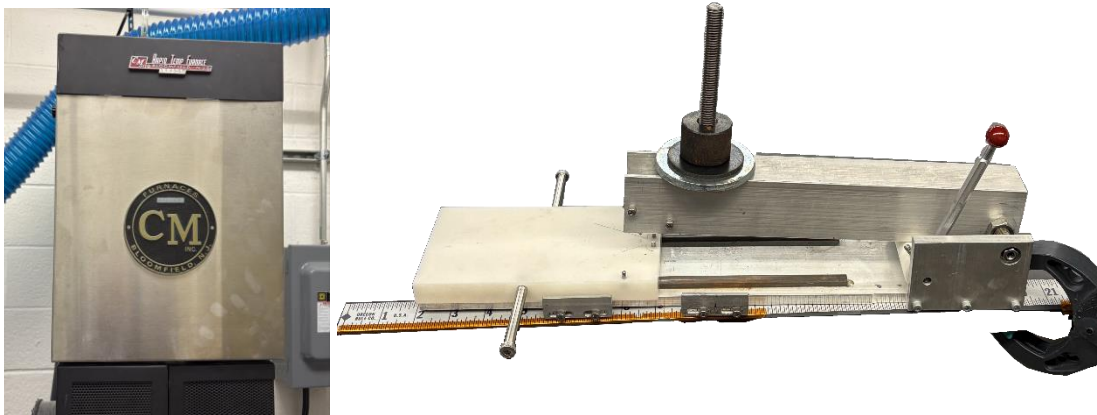


Figure 5. CM Furnace 1218BL; Luna scribing device, clamped to table

Results

Chromium-based IPcote vs. Zinc Clad Surface Topography.

The surface topography of the SW coating appeared like typical IOZ (inorganic zinc) coatings (Figure 6a). The zinc particles are spherical, with the silicate material filling in gaps with more irregular shapes.

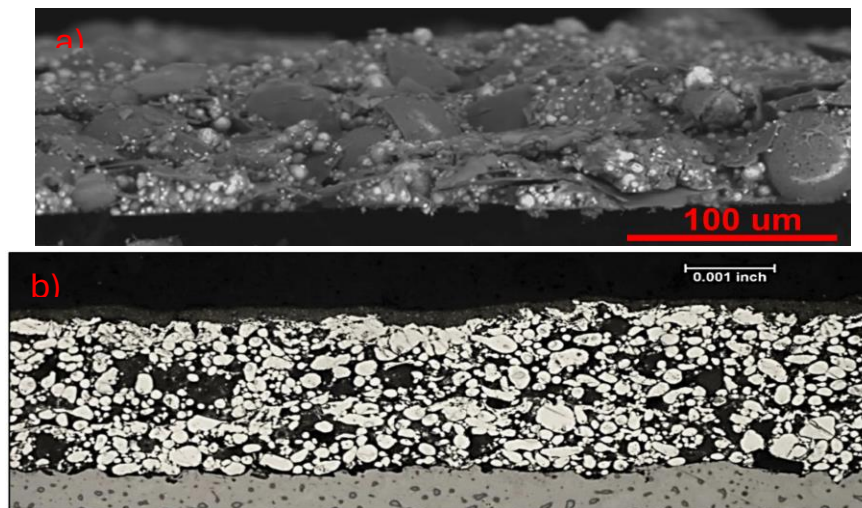


Figure 6. Surface topography (a) of an unnamed Jotatemp IOZ coating (Jotun, n.d). Rolls Royce publication (b) showing cross section of IPcote 9183R1 coating (Wiley, 2022).

Images of coupons immediately after applying sol-gel coatings with HVLP spray, before curing of sol-gel coatings, can be seen in the figure below. Images of SAE 4340 steel coated with IPcote are included in this figure for direct comparison with the control—the substrate is 4340 for IPcote samples because they are leftovers from a RR project.

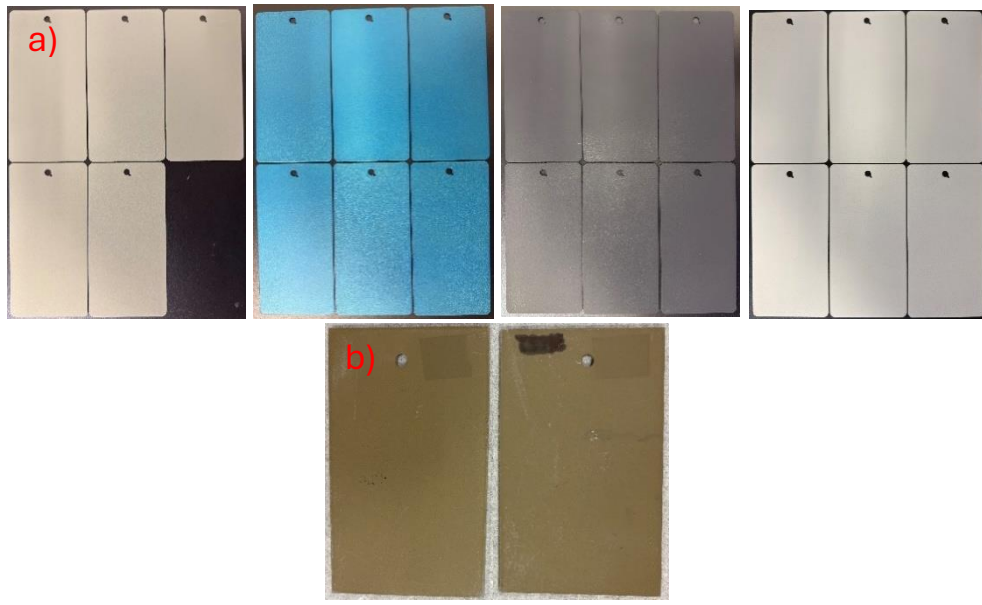


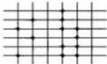
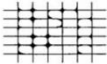
Figure 7. (a) Substrate appearance directly after sol-gel application (before sol-gel curing); (b) IPcote samples sent by RR.

Coating Adhesion and Blistering.

All coatings experienced adhesion issues. To rank or quantify adhesion, ASTM D3359 was conducted on the thermally screened sample from each group (Figure 7). ASTM D3359 crosshatch adhesion testing was done to the SW base coat, for which the adhesion rating was the lowest on the scale: 0B (Table IV). Complete delamination of ZC can be seen in Figure 8a.

Table IV. ASTM D3359 crosshatch adhesion scale.



Classification	Surface of cross-cut areas from which listing has occurred. (Example for six parallel cuts.)	Rate of adhesion
5B	None	The edges of the cuts are completely smooth; none of the squares or the lattice are detached.
4B		Small flakes of coating are detached at intersections; less than 5% of the area is affected.
3B		Small flakes of coating are detached along edges and at intersections of cuts. The area affected is 5 to 15% of the lattice.
2B		The coating has flaked along the edges and at parts of the squares. The affected area is 15 to 35% of the lattice.
1B		The coating has flaked along the edges of cuts in large ribbons and entire squares have detached. The area affected is 35 to 65% of the lattice.
0B	Flaking and detachment in excess of 65%.	

ASTM D714-25 was used to evaluate the degree of blistering experienced by the topcoat of this panel. The standard leverages references to help determine the size and frequency of the blisters. Size is on a scale from 10 to 0, with No. 10 referring to no blistering. Size 8 blisters are the smallest on the scale that can be seen macroscopically (ASTM, 2025). The frequency is on step wise scale going few to dense. ZC only featured no blistering before salt fog, however, prominent blisters formed while the coupons were in the salt fog which can be seen in the Appendix. The resulting blisters are size 2 with a distribution of a few.

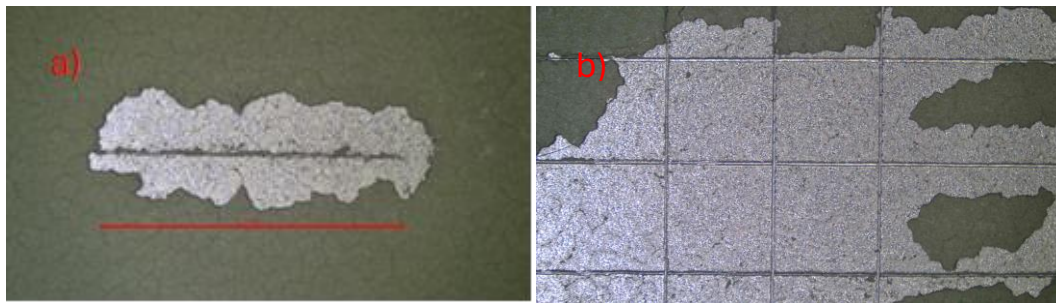


Figure 8. Scribe adhesion testing (a) and ASTM D3359 (b) crosshatch adhesion testing of ZC base coat.

There was also significant cracking in the ZC-only coating (Figures 8 and 9b). In the SEM, spherical, light particles of zinc contrast with the dark, more irregular pieces of silicate-based material (Figure 9a).

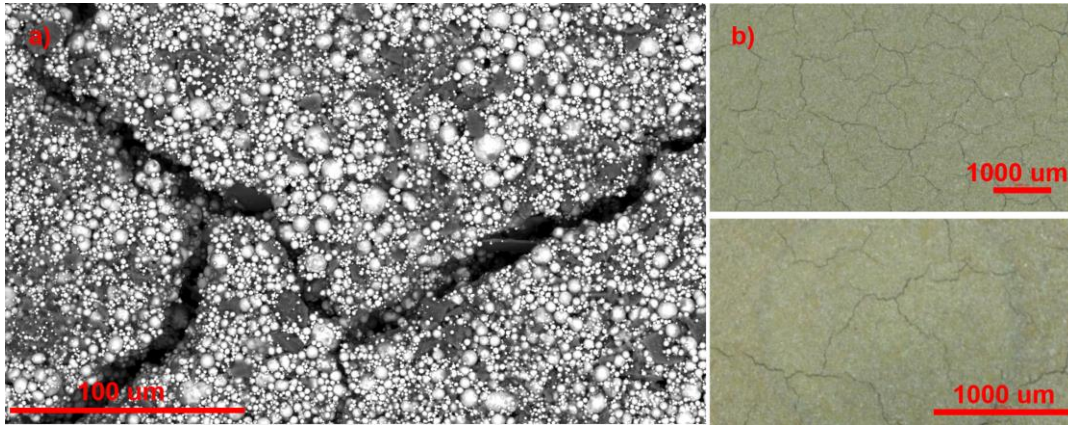


Figure 9. ZC-only coupon surface view from (a) SEM at 1650x and (b) light microscope.

Luna added blue pigment to the HTB1 coating, giving it the most distinct appearance of the topcoats. Between Figures 10 and 8a, adhesion improvement from 0B to 1B can be seen. The 1B rating indicates that “the coating has flaked along the edges of cuts in large ribbons and whole squares have detached; the area affected is 35 % to 65 % of the lattice” (ASTM, 2023). HTB1 also featured no blistering, therefore giving it a rating of 10.



Figure 10. ASTM D3359 crosshatch adhesion test of HTB1 coating matrix.

Meanwhile, the HTB2 coating was initially black with zinc metal flakes embedded (Figure 11). The poor adhesion of this topcoat was the same as the SW only sample, a 0B on the ASTM D3359 scale. There was also no blistering on the surface of the panel.



Figure 11. ASTM D3359 crosshatch adhesion test of HTB2 coating matrix.

HTB3 had white pigment, extremely small blisters on its surface, and out of all topcoats performed the best in adhesion testing. According to ASTM D714-25, the blisters can be classified as a size 9 with a dense distribution across the panel. Its 2B rating indicates that “the coating has flaked along the edges and on parts of the squares; the area affected is 15 % to 35 % of the lattice” (ASTM, 2023).

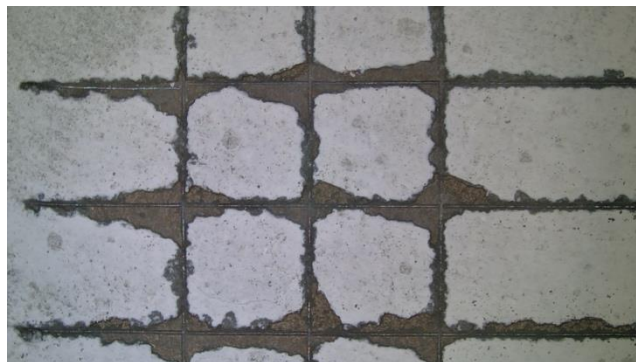


Figure 12. ASTM D3359 crosshatch adhesion test of HTB3 coating matrix.

Slightly more yellow-white than HTB3, the HTB4 group had extreme blistering and deep mud cracking. While similar pore and crack patterns appeared in HTB3 and HTB4, no deep cracks appeared in the HTB3 coating. HTB3 pores were also far less developed. Based on ASTM D714-24, the blisters on HTB4 can be classified as size 8, with a medium-dense distribution across the coupon surface. With its crosshatch adhesion rating of 1B, HTB4 adhesion was significantly better than ZC-only and HTB2, but not as good as HTB3. (Figure 13)

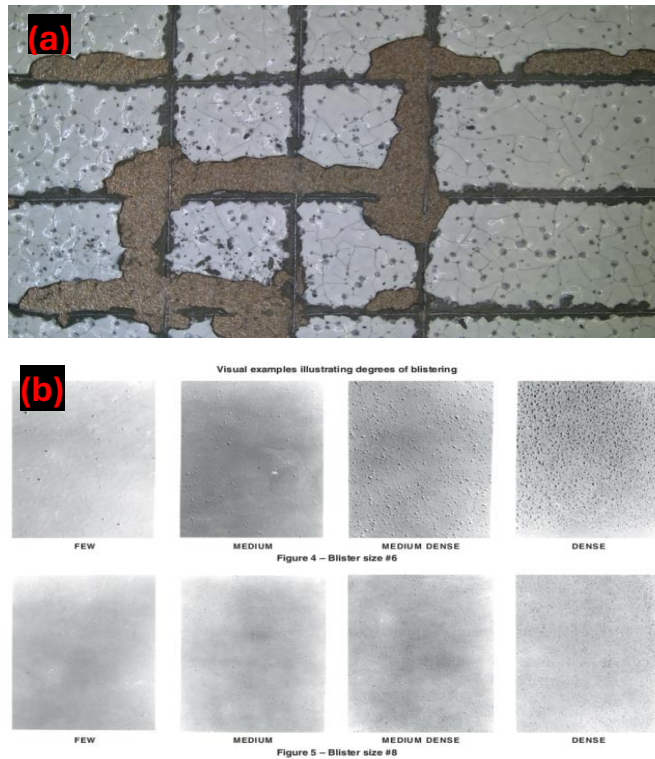


Figure 13. (a) ASTM D3359 crosshatch adhesion test of HTB4 coating matrix and ASTM D714
 (b) blistering scale.

The chromium-based IPcote cracked in a more angular manner than ZC only and ZC-based matrices. EDS helped the team determine that the IPcote was a two-component system: the flat areas in Figure 14 were the aluminum-containing base coat, while the top seal contained chromium and phosphorus. Wiley confirmed the sealant to have a polymeric base derived from phosphoric and chromic acid.

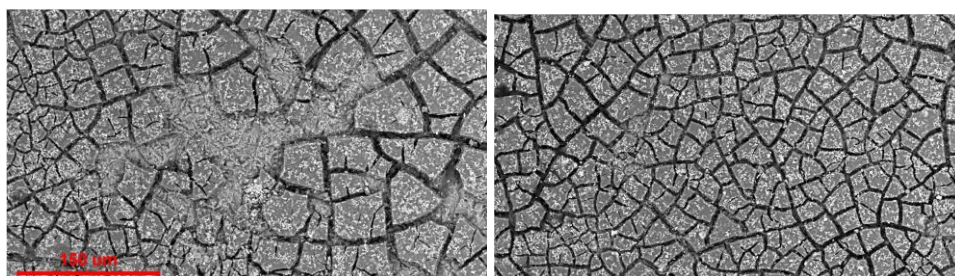


Figure 14. HC coupon surface view from SEM at 1000x.

Thermal Screening.

Temperatures for final isothermal holds were determined based on which screening test showed the least evidence of microcracking and adhesion loss. Recommended thermal exposure temperatures can be found in Table V.

ZC-only hardness increased as screening temperature increased. However, thermal screening also revealed how poorly the Zinc Clad II Plus adheres to the AISI 1010 substrate by itself. Fortunately, the addition of the HTB topcoats seemed to prevent the ZC from peeling off from the substrates as quickly. (Figure 15)

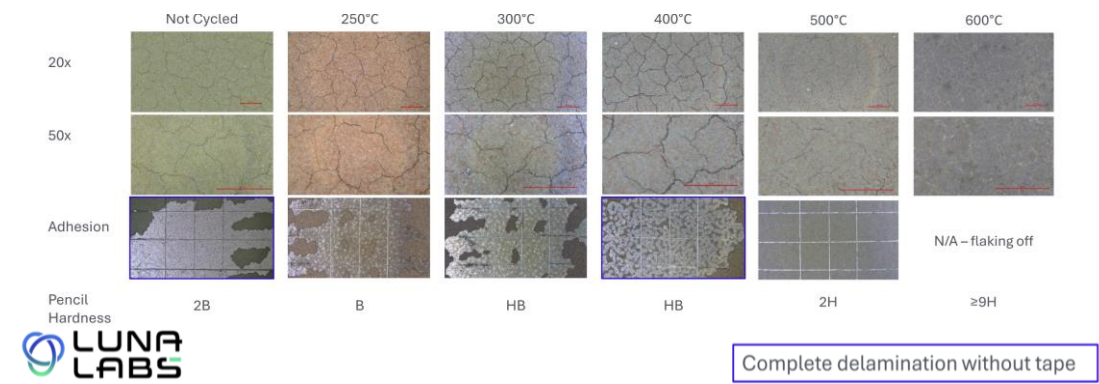


Figure 15. ZC-only coating surface and adhesion testing after thermal cycling.

High temperatures induced similar microcracking patterns throughout the HTB coatings. The HTB3 had the best macroscopic appearance at higher temperatures, resulting in this group having the highest recommended temperature: 400°C. Moreover, significant microcracking only began at 500°C. However, since the HTB3 lost adhesion at 400°C and adhesion loss temperature was more important in determination of the isothermal hold temperatures, the recommended temperature was set to the lower bound of 400°C. For HTB2 and HTB4, microcracking began at 300°C; the HTB1 group began to crack immediately in the 250°C hold. Complete sets of micrographs for all lower temperature combinations—HTB1, HTB2, and HTB4—can be found in the appendix. (Figure 16)

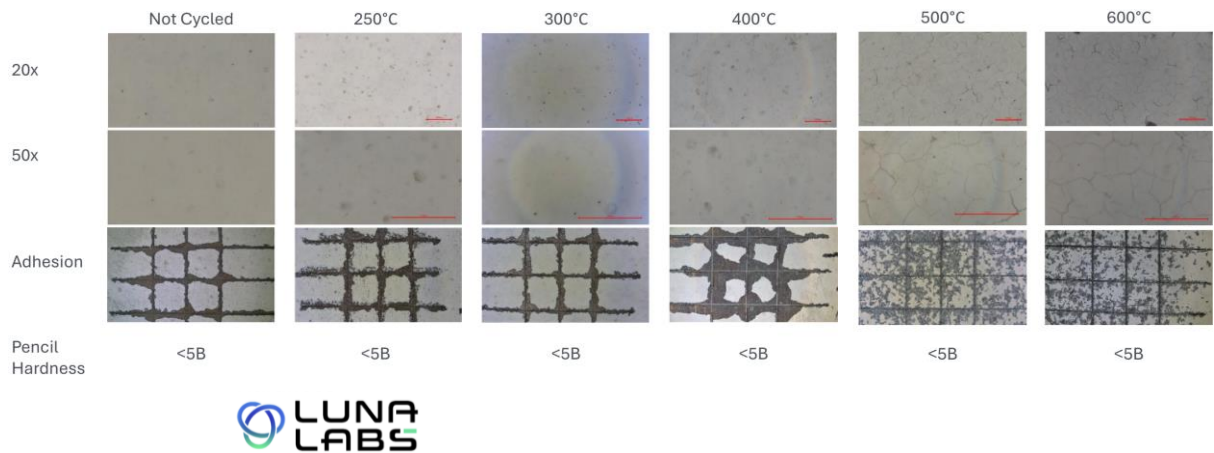


Figure 16. ZC+HTB3 thermal screening

Table V summarizes temperatures at which microcracking, adhesion loss, and hardness loss each first appeared. Luna Labs reported that the ZC-only sample was the only one that showed an increase in hardness after thermal screening. Interestingly, both the HTB2 and HTB4 sets experienced an improvement in adhesion with an increase in temperature. However, due to Luna trade secrets, further analysis of this in relation to coating composition will be difficult.

Table V. Thermal screening results.

Coating(s)	Microcracking Temperature (°C)	Adhesion Loss Temperature (°C)	Hardness Loss Temperature (°C)	Recommended Group Temperature (°C)
ZC Only	500	N/A*	N/A*	500
ZC + HTB1	250	N/A	300	200
ZC + HTB2	300	400*	400	300
ZC + HTB3	500	400	N/A	400
ZC + HTB4	300	250*	400	300

*Improvement seen at higher temperatures

Isothermal Holds.

From April 1st to the 4th, the five primary substrates in each group were held at their recommended temperatures. No significant differences in performance were seen between screening and official isothermal holds. Images from before salt fog testing and after isothermal holds will be included here.

Salt Fog Testing.

White streaks increased across the HTB1 sample with increased exposure to salt fog. A white film developed across the scribe area. The second coupon in the testing group developed a chipped area in the internal section of the scribe. This was a product of the scribing and masking process. No macroscopic red rust appeared over the recorded exposure periods; very few specks of rust appeared in scribes. (Figure 17)

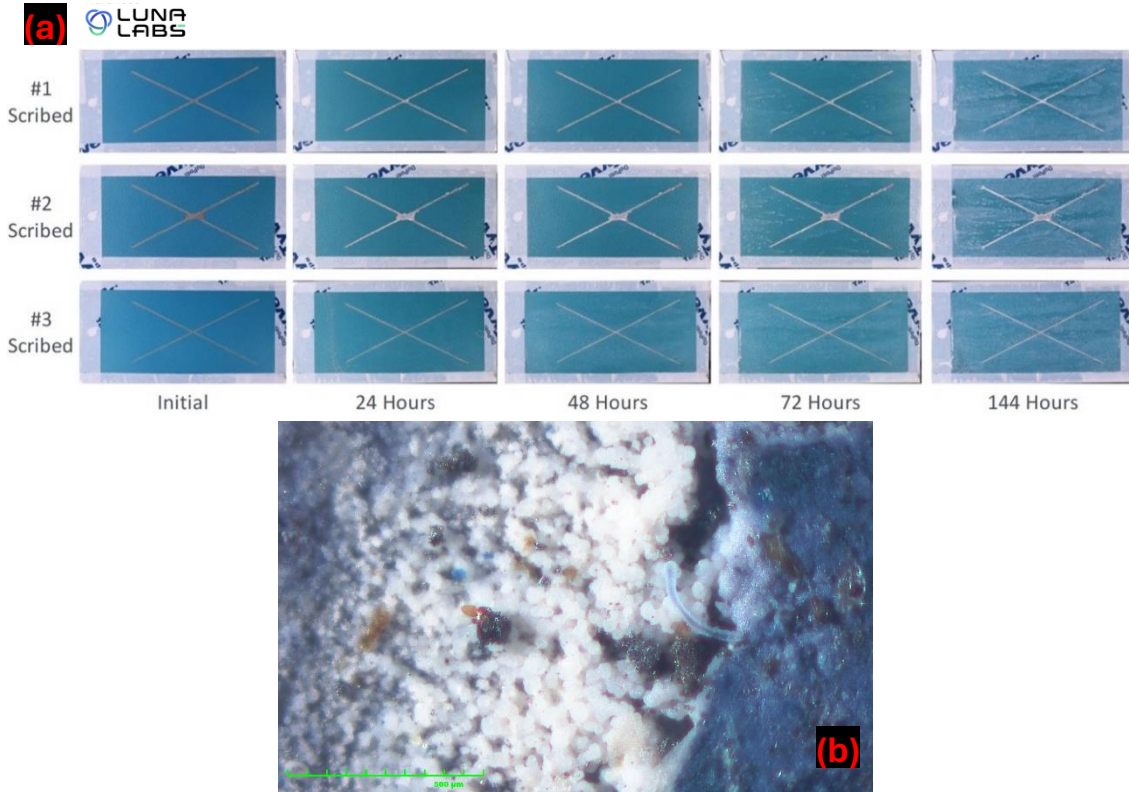


Figure 17. (a) ZC+HTB1 after 200°C hold and salt fog testing (Luna, 2025); (b) 150X Hirox micrograph showing red rust in scribe.

White streaks also developed across the HTB2 samples, in Figure 18, which appear thicker than on the HTB1 samples. Large regions of the film that developed on this coupon group took on a faintly orange hue—red rust almost as pervasive in the HTB2 samples as the ZC-only. (Figure 18)

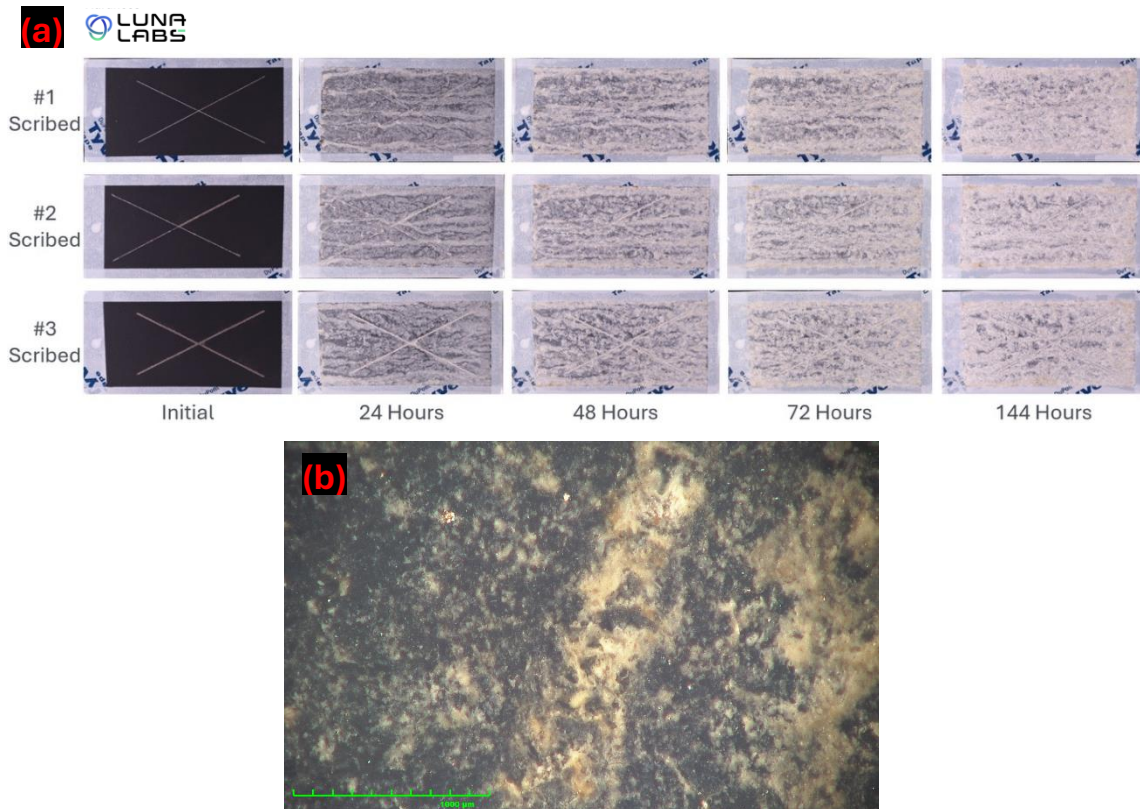


Figure 18. (a) ZC+HTB2 after 300°C hold and salt fog testing (Luna, 2025); (b) 100X Hirox micrograph of HTB2 scribe.

Corrosion products on the HTB3 group are difficult to see in macro-scale images due to the coating being white. While no red rust could be seen macroscopically, small spots of red rust could be seen at higher magnifications under the Hirox Light Microscope (Figure 19).

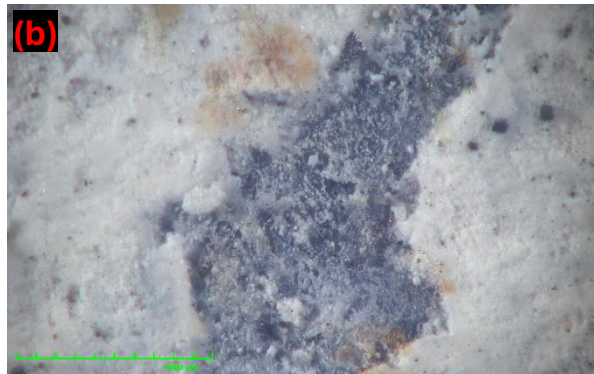
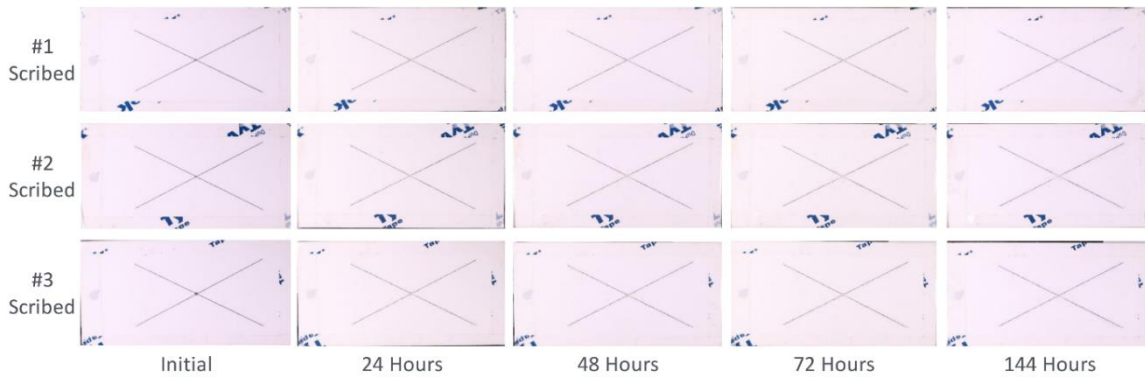


Figure 19. (a) ZC+HTB3 after 400°C hold and salt fog testing (Luna, 2025); (b) 100X Hirox micrograph of HTB3 scribe.

In macroscopic HTB4 images, red rust can be seen around the scribe. Microscopically, mud cracking and large divots are pervasive; even away from the scribe, red rust can be seen in mud cracks. (Figure 20)

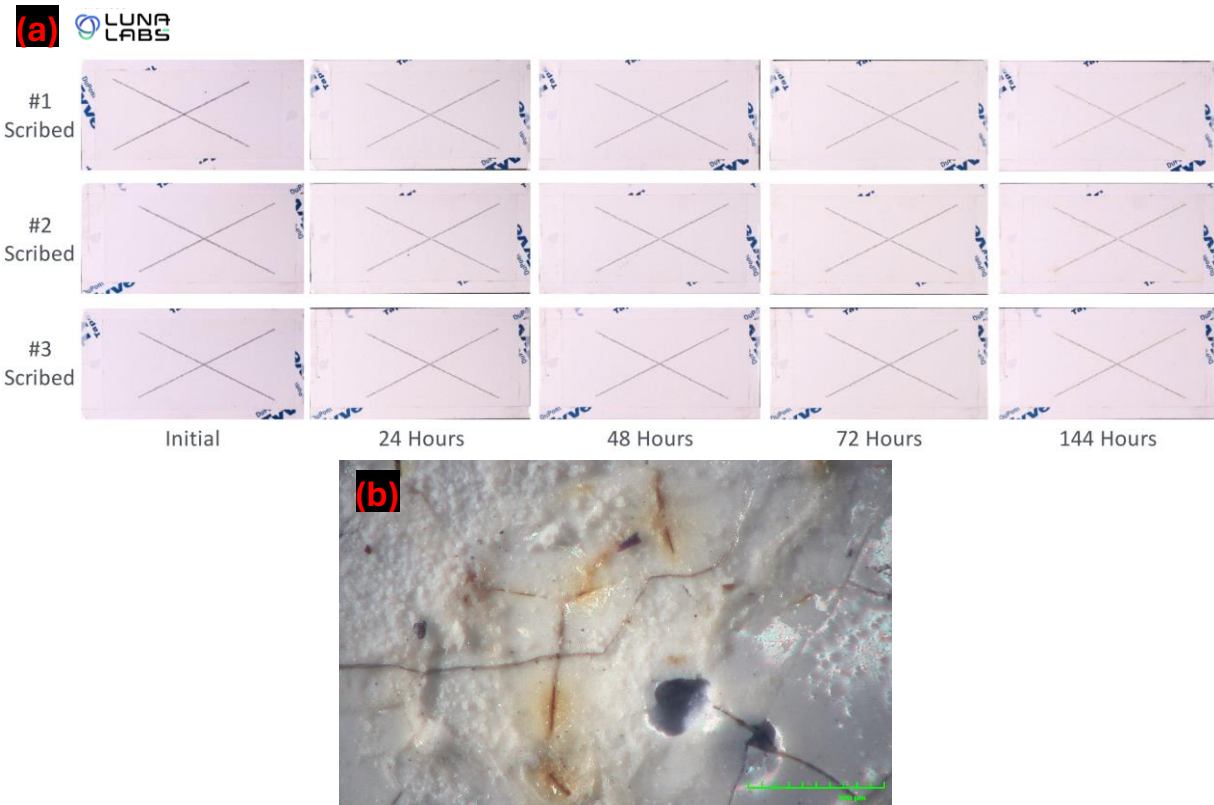


Figure 20. (a) ZC+HTB4 after 300°C hold and salt fog testing (Luna, 2025); (b) 150X HTB4 Hirox micrograph.

Rust analysis was conducted by increasing the contrast of coupon images and averaging the number of spots across the two unscribed coupons. Since ASTM D610-08 appears to only quantify rust on unscribed samples, the two unscribed coupons from each group were analyzed. No figure for HTB1 was included because no rust being macroscopically visible on unscribed coupons. As HTB2 completely delaminated, performing worse than the ZC-only (when comparing unscribed samples), it was too difficult to determine individual spots of rust. The average quantity of rust spots across the two unscribed ZC-only samples was 74 (Figure 21).

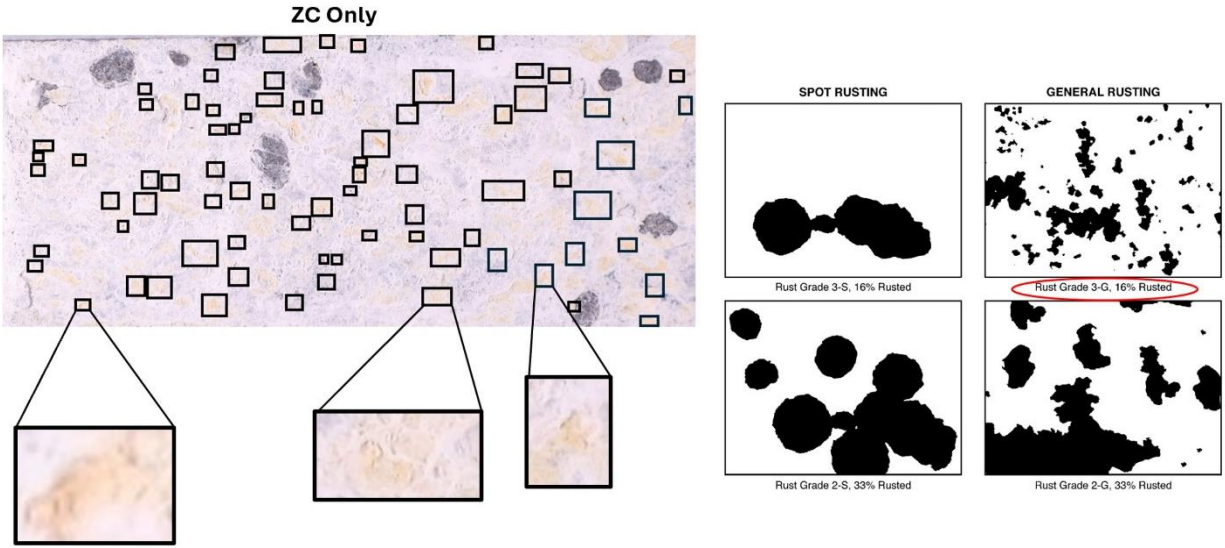


Figure 21. ASTM D610-08 for ZC Only. General rust count inside the boxes: 74.

ASTM D610 only worked to quantify spots of rust on HTB3 and HTB4 samples: on HTB3 samples, small spots of rust appeared, while HTB4 had larger regions of red rust that appeared with slightly less frequency (Figure 22).

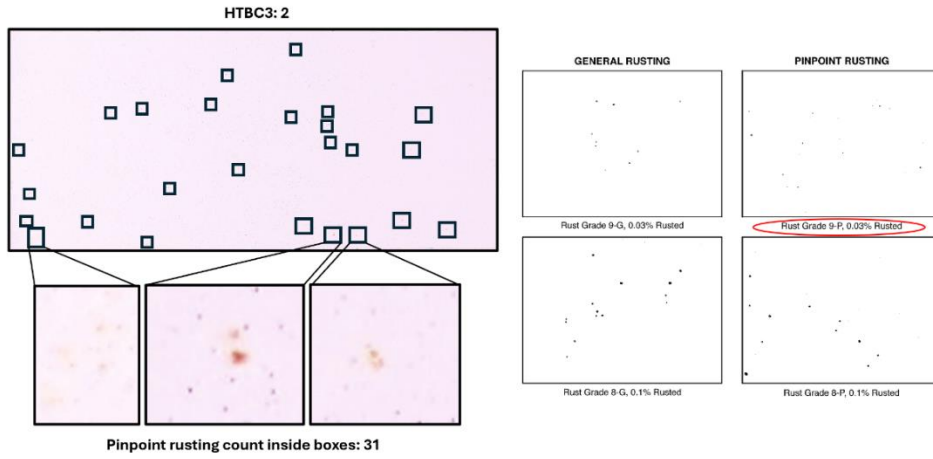
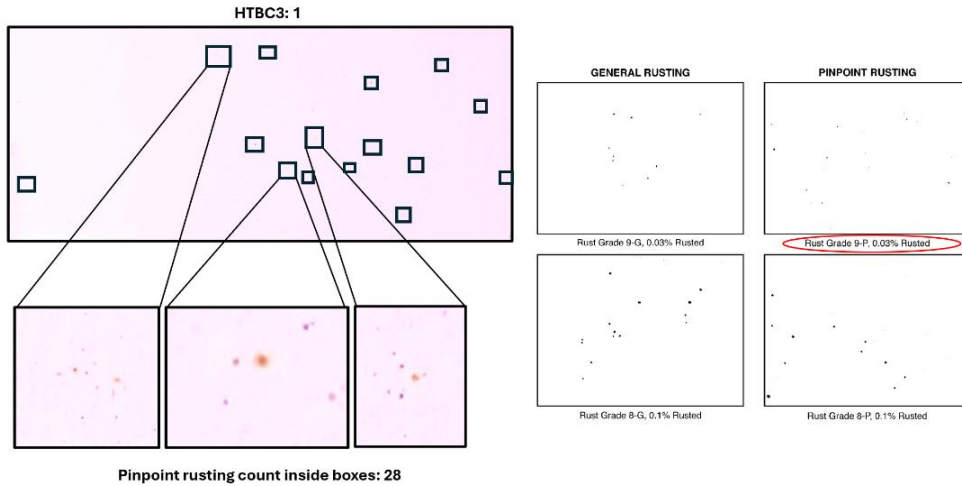
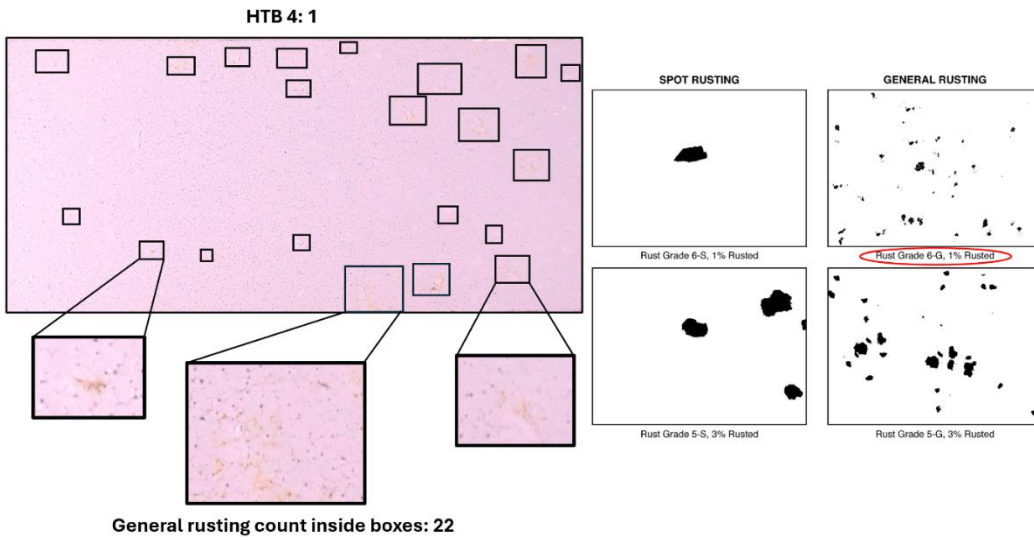


Figure 22. ASTM D610-08 for HTB3, from two different substrates. The average number of rust spots is 29.



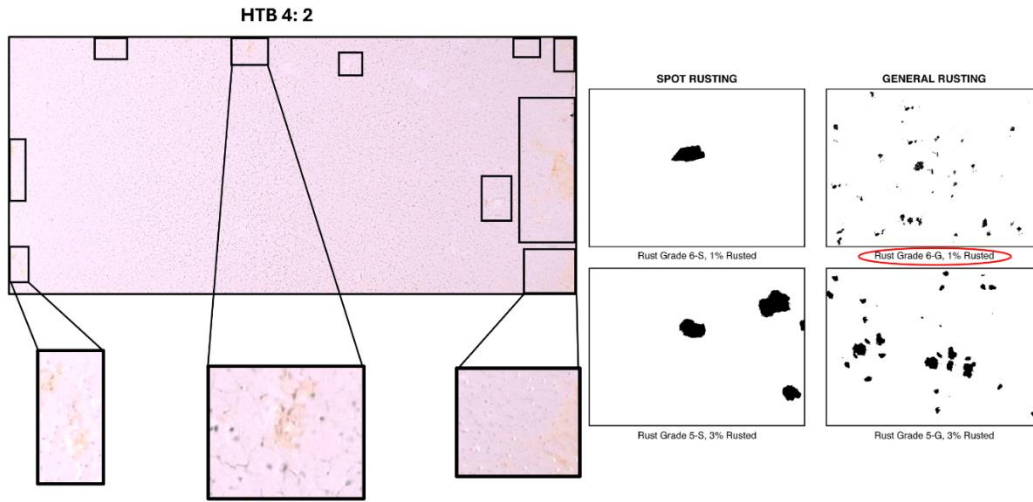


Figure 23. ASTM D610-08 for HTB4, from two different substrates. The average number of rust spots is 16.

Discussion

Zinc Clad II Plus Overcoating.

Most issues in the results arose from SW having applied too thick a layer of Zinc Clad to substrates. Luna Labs measured the ZC base coat to be 8-10 mils; SW specifications denote that typical ZC application should be 2-3 mils. The cracks in HTB1, HTB3, and HTB4 samples shown below, a well-known phenomenon called mud cracking, are all caused by overcoating. These cracks “resemble the appearance of a dried-up riverbed during a severe drought” (*Chemistry and Physics of Coatings*, 2004). Adhesion issues with ZC seemed to affect HTB topography, reducing the thermal barrier capabilities of HTB variants, but HTB4 in particular—the HTB thermal barrier coatings would ideally coat samples uniformly. Any cracking in barrier coatings severely reduces coating protection. When asked to confirm if the overcoating was intentional, Sherwin Williams said that the coating should have been in the range of two to three thousandths of an inch.

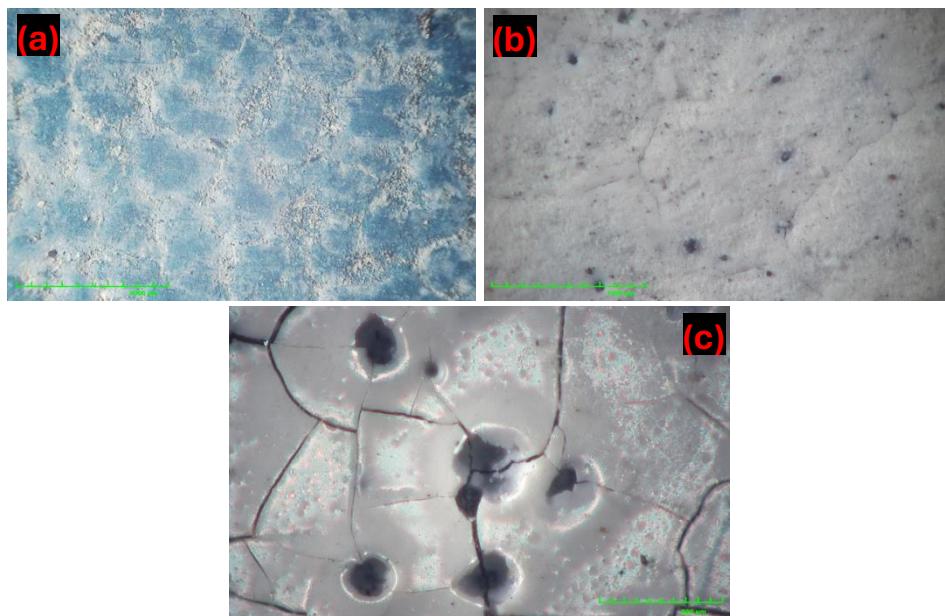


Figure 23. Mud cracking in different HTB-coated samples: (a) HTB1 at 100X, (b) HTB3 at 100X, (c) HTB4 at 150X.

The curing of the ZC coating for adhesion testing prior to thermal exposure could have caused adhesion loss. Adhesion is usually not an area of concern for IOZ coatings, as interactions between zinc ions, solvent, and the steel substrate typically bind the coating to the steel surface. However, dry climates can markedly reduce cure rate—high humidity is necessary because curing rate of alkyl silicates depends heavily on relative humidity. (Parashar, 2001)

The corrosion performance of Zinc Clad typically observed by Luna Labs, where the Zinc Clad does not experience cracking, can be attributed to the reaction of zinc with corrosive environments. Over time, more and more corrosion products—inert compounds from zinc reacting with the environment—build up in cracks, resulting in greater corrosion resistance. The zinc sacrificially corrodes to protect the substrate from damage, providing barrier protection inside coating cracks and voids. Silicate polymers reinforce the barrier protection created by the zinc-environment reactions. (Francis, 2013).

Zinc Clad is an ethyl silicate, solvent-based IOZ coating. At higher temperatures, ethyl silicate has been observed to increase in hardness (Ali, 2012). Zinc Clad hardness increasing at higher temperatures could have been initiated by the ethyl silicate within it hardening at higher temperatures (Ali, 2012). Strengthening could be attributed to crosslinking, which would also explain the other phenomena seen on some of the coatings: cracks on the surfaces of the ZC-based coupons before and after the thermal screening. Greater amounts of crosslinking have been attributed to increased IOZ coating brittleness.

Degree of Rusting on Un-Scribed Coupons from Salt Fog

All the unscribed coupons except for the ZC scored the lowest rust grade for their identified rust type. The HTB3 showed pinpoint rusting while the HTB4 showed general rusting. The difference in rust types could be attributed to the difference in composition between the two HTB groups. The performance of the ZC could be attributed to the thermal exposure temperature it was exposed to, which was beyond the recommended level recommended by Sherwin Williams and above the melting point of zinc around 400°C. The inconclusive HTB2 results in a lack of understanding for the rusting behavior of that group. The HTB1 showed no level of red rust, which makes it an optimal coating at that coating temperature.

Rust Undercutting in Scribed Coupons from Salt Fog

The only coupon that showed undercutting was the HTB3 returned to the team after salt fog testing, which can be seen in Figure A8 in the appendix. It was in only one area, and the rest of the HTB and ZC coating remained intact across the substrate. This could mean that the HTB adhered to the ZC coating better than the substrate at that area as well as that the ZC curing at that area didn't develop an iron-silicon-zinc matrix. All other coupons were unable to have their coatings removed near the scribes for undercutting analysis. This could be related to the influence of heat on IOZ coatings, which would have commenced during thermal screening and

exposure. When exposed to heat, the interface between the steel and IOZ coating can develop an iron-zinc-silicon matrix that allows for adhesion of the coating to the substrate (Francis, 2013). The lack of adhesion before any thermal test and adhesion after thermal exposure supports this.

Sol-Gel Barrier Coatings.

Sol-gels are currently at the forefront of initiatives to create nontoxic coatings and pretreatments for metal. Widely classified as a form of nanotechnology, sol-gels find use in areas such as ceramic molds, biomedical and piezoelectric devices, and protective thin-films (Owens et al., 2016; Bokov et al., 2021). Advantages of sol-gels include their high purity, homogeneity, and moreover, reaction kinetics can be adjusted to fine-tune sol-gel properties (Dmitriev et al., 2008). Since sol-gels can be created at room temperature, they are more cost-effective to manufacture on a large scale compared to the other high-temperature methods of thin-film creation (Kate et al., 2018). Room-temperature synthesis also means entrapped corrosion inhibitors experience less degradation (Figueira, 2020). Homogenous thin-films created with the sol-gel process function well as barrier coatings, which is why the team sought out a sol-gel topcoat (Gichuhi et al., 2009). Ingredients of Luna sol-gel coatings cannot be discussed in this paper due to company trade secrets.

The ability to adjust each reaction in the sol-gel process makes this technology extremely versatile. To form a sol-gel, an inorganic metal alkoxide or metal chloride starter called a precursor¹ first undergoes hydrolysis and condensation to create a colloidal² suspension, or sol (Singh et al., 2014). A colloidal suspension is composed of 1-100nm solid particles suspended in a liquid. Hydrolysis rate depends on the precursor involved, which in turn affects the properties of the product. This colloidal suspension goes through more condensation to become a gel. The gel has a porous, rigid network of polymeric chains; these pores trap solvent (Tao & Pescarmona, 2018). The gel will be wet after condensation, so it must either be air-dried (to produce a xerogel) or dried with supercritical carbon dioxide (to become an aerogel³). HTB coatings were cured in

¹ “...extensively used precursors are tetramethoxy [silane](#) and tetraethoxy [silane](#).” (Singh et al., 2014)

² The definition of a colloid from [Eric Lee](#): “A colloidal particle is a small particle with dimension scale ranging from [nanometers](#) to micrometers, depending on the specific colloidal behavior under consideration. For instance, the upper bound has to be smaller than about five micrometers if the stability of a [colloidal suspension](#) is of concern, as beyond this limit the Brownian motion of the particles may not be strong enough to keep them from coagulation with one another.”

³ Drying the gel in supercritical carbon dioxide better preserves a porous structure, making for lighter material and fast water uptake. The paper cited in this footnote discusses aerogels in biomedical applications, as porosity is important in biocompatible and biodegradable materials. Aerogels are also used in energy storage and catalysis. ([Machado et al., 2025](#))

air. Included in the figure below are chemical reactions for each step in the process. (Singh et al., 2014 & Aurobind et al., 2006)

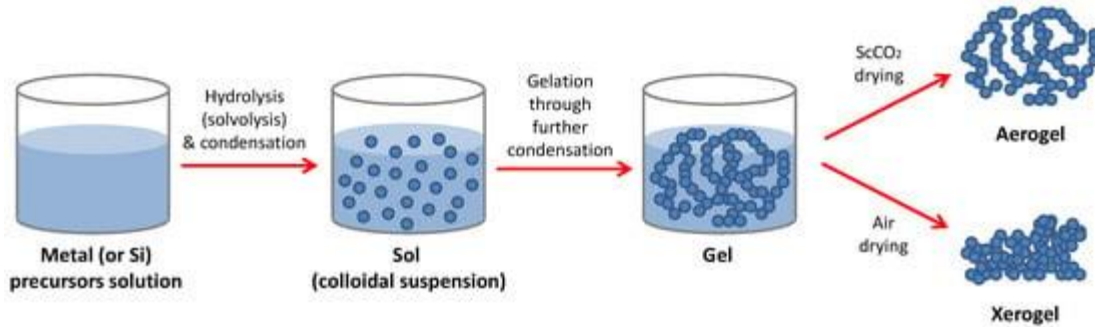
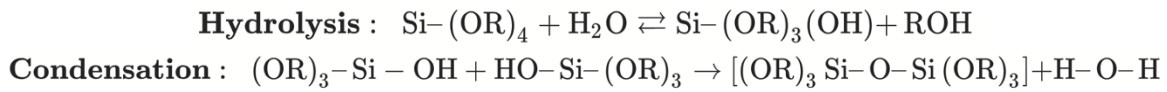


Figure 23. Sol-gel reactions (above); diagram of sol-gel synthesis (below). (Singh et al., 2014; Tao & Pescarmona, 2018)

Oxygen cannot diffuse easily through sol-gel coatings, giving them high oxidation resistance (Durán et al, 2007). In addition to this, doping sol-gel coatings with inhibitors slows gelation, reinforcing protection against oxidation (Durán et al, 2007). Inhibitor-doped sol gel coatings “[form] a protective coating in situ by reaction of the solution with the corroding surface” (Jones, 1996). This layer protects the coating by suppressing polarizing electrochemical reactions over both anodic and cathodic regimes (Jones, 1996). The behavior of Luna HTB coatings indicates that they are likely doped with inhibitors, as the barrier coatings are still somewhat present after salt fog results.

Conclusions and Future Work

The HTB3 coating combination survived at the highest temperature and exhibited the least red rust of the samples. Though less rust and blistering appeared on the HTB1 samples, its lower temperature resistance means it ranks second when considering resistance to salt fog and thermal corrosion. After this project, Luna Labs will continue to monitor the salt fog performance of these HTB variations for their own research, checking when coupons begin to exhibit red rust, coating delamination, and severe discoloration. Since this screening was conducted on new coatings at a low technology readiness level (TRL), higher TRL testing—such as in coastal areas or on a seafaring aircraft carrier—would be needed to determine whether one of these coating matrices could survive in more realistic conditions and on more complex geometries, with the ultimate goal of surviving application inside a turbine engine.

Future studies of other sol-gel coatings could include adjusting existing high-temperature sol-gel formulations by adding corrosion inhibitors. Alternatively, the effect of applying sol-gels with dip coating versus HVLP spray could be studied—literature mentions that dip coating tends to be more common (Durán et al, 2007). The thermal limits of ZC could also be closely studied, since isothermal screening revealed ZC begins to fail when held at 500°C.

This project has effectively screened the proposed two-part coating systems created in conjunction with industry partners. However, because this project only screened new coating matrices and samples hardly survived at half the maximum temperature hexavalent chromium does, it is only possible to suggest how to move forward with testing: no coating combination tested here currently stands as a replacement for hexavalent chromium coatings.

Acknowledgements

We would like to thank Brad Wiley and Rob Golden at Rolls Royce for giving us the initial proposal for the project as well as providing guidance throughout. We hope that our findings can be used to develop more alternatives to hex-chrome.

We are indebted to Dr. Rebecca Marshall, Adam Goff, and the whole team at Luna Labs for allowing us to use their facilities, products, and labor at no additional cost. They fielded any questions that we had and gave us constant guidance.

We would also like to thank Dr. Robert Kelly for the time he took out of his schedule to be our subject matter expert. His guidance and humor helped carry us past roadblocks throughout the design process.

To our capstone advisor Dr. Jim Fitz-Gerald, we extend our sincerest gratitude for the constant guidance and reassurance he supplied over the year, and for teaching us the tools necessary to make this project successful.

For sectioning our samples in the SEM and being so patient as we felt our way through this process, we would like to thank Tanner Fitzgerald.

Finally, we would like to thank the Materials Science department for bringing us together and covering all costs for the project.

References

- Ali, M., Mohammed, J., Zainulabdeen A., et al. (2021). Experimental study of the mechanical and corrosion properties of ethyl silicate resin applied on low carbon steel. *Archives of Materials Science and Engineering*, 108(2), 68-74. <https://doi.org/10.5604/01.3001.0015.0255>.
- ASTM. (2019a, January 7). *Standard practice for evaluating degree of rusting on painted steel surfaces*. ASTM International. <https://store.astm.org/d0610-08r19.html>
- ASTM. (2019b, January 7). *Standard test method for evaluation of painted or coated specimens subjected to corrosive environments*. ASTM International. <https://store.astm.org/d1654-24.html>
- ASTM. (2019c, December 10). *Standard practice for operating salt spray (fog) apparatus*. ASTM International. <https://store.astm.org/b0117-19.html>
- ASTM. (2023, March 7). *Standard test methods for rating adhesion by tape test*. ASTM International. <https://store.astm.org/d3359-23.html>
- ASTM. (2025, January 28). *Standard test method for evaluating degree of blistering of paints*. ASTM International. <https://store.astm.org/d0714-02r17.html>
- ATSDR. (2023, May 24). *Chromium (Cr) Toxicity: What are the Physiologic Effects of Chromium Exposure?*. Agency for Toxic Substances and Disease Registry (ATSDR). https://www.atsdr.cdc.gov/csem/chromium/physiologic_effects_of_chromium_exposure.html
- Aurobind, S. V., Amirthalingam, K. P., & Gomathi, H. (2006). Sol-gel based surface modification of electrodes for electro analysis. *Advances in Colloid and Interface Science*, 121(1), 1–7. <https://doi.org/10.1016/j.cis.2006.04.001>
- Chemistry and Physics of Coatings*, edited by Alistair R. Marrion, The Royal Society of Chemistry, 2004. *ProQuest Ebook Central*.
- Davis, J. R. (2000). *Corrosion: Understanding the basics*. ASM International.
- Durán, A., Castro, Y., Aparicio, M., Conde, A., & de Damborenea, J. J. (2007). Protection and surface modification of metals with sol–gel coatings. *International Materials Reviews*, 52(3), 175–192. <https://doi.org/10.1179/174328007X160263>
- Figueira, R. B. (2020). Hybrid Sol–gel Coatings for Corrosion Mitigation: A Critical Review. *Polymers*, 12(3), 689. <https://doi.org/10.3390/polym12030689>

- Francis, R. (2013). Inorganic zinc silicate coatings: Fallacies and facts. *ACA Corrosion & Prevention, Brisbane*.
- Guglielmi, M. Sol-Gel Coatings on Metals. *Journal of Sol-Gel Science and Technology* **8**, 443–449 (1997). <https://doi.org/10.1023/A:1018373404815>
- IARC Working Group on the Evaluation of Carcinogenic Risks to Humans. (1990) *Chromium, Nickel and Welding*. Lyon (FR): International Agency for Research on Cancer; (IARC Monographs on the Evaluation of Carcinogenic Risks to Humans, No. 49.) CHROMIUM AND CHROMIUM COMPOUNDS.
- Jones, D. A. (1996). *Principles and Prevention of Corrosion* (2nd ed.). Upper Saddle River, NJ: Prentice Hall.
- Jotun. (n.d). *The challenges facing zinc silicates at high temperatures – part 1*. Retrieved from <https://www.jotun.com/ww-en/industries/solutions-and-brands/jotatemp/resources/the-challenges-facing-zinc-silicates-at-high-temperatures-part-1>
- Kate, R. S., Khalate, S. A., & Deokate, R. J. (2018). Overview of nanostructured metal oxides and pure nickel oxide (NiO) electrodes for supercapacitors: A review. *Journal of Alloys and Compounds*, *734*, 89–111. <https://doi.org/10.1016/j.jallcom.2017.10.262>
- Mustafa, G., Li, B., & Zhang, S. (2024, February 1). Cutting condition effects on microstructure and mechanical characteristics of Ni-based superalloys—a review. *International Journal of Advanced Manufacturing Technology*, *130*(7/8), 3179 - 3209. Retrieved from <https://doi.org/10.1007/s00170-023-12910-z>
- Hexavalent Chromium*. (n.d.). National Institute of Environmental Health Sciences (NIEHS). Retrieved May 7, 2025, from <https://www.niehs.nih.gov/health/topics/agents/hex-chromium>
- Owens, G. J., Singh, R. K., Foroutan, F., Alqaysi, M., Han, C.-M., Mahapatra, C., Kim, H.-W., & Knowles, J. C. (2016). Sol–gel based materials for biomedical applications. *Progress in Materials Science*, *77*, 1–79. <https://doi.org/10.1016/j.pmatsci.2015.12.001>
- Parashar, G., Srivastava, D., & Kumar, P. (2001, January 1). Ethyl silicate binders for high performance coatings. *Progress In Organic Coatings*, *42*(1), 1 - 14. Retrieved from [https://doi.org/10.1016/S0300-9440\(01\)00128-X](https://doi.org/10.1016/S0300-9440(01)00128-X)
- Francis, R. A. (2013). Inorganic Zinc Coatings: History, Chemistry, Properties, Applications and Alternatives.

- Shin, D. Y., Lee, S. M., Jang, Y., Lee, J., Lee, C. M., Cho, E.-M., & Seo, Y. R. (2023, February 8). *Adverse Human Health Effects of Chromium by Exposure Route: A Comprehensive Review Based on Toxicogenomic Approach*. U.S. National Library of Medicine. <https://www.ncbi.nlm.nih.gov/pmc/articles/PMC9963995/>
- Singh, L. P., Bhattacharyya, S. K., Kumar, R., Mishra, G., Sharma, U., Singh, G., & Ahalawat, S. (2014). Sol-Gel processing of silica nanoparticles and their applications. *Advances in Colloid and Interface Science*, 214, 17–37. <https://doi.org/10.1016/j.cis.2014.10.007>
- Tao, Y., & Pescarmona, P. P. (2018). Nanostructured Oxides Synthesised via scCO₂-Assisted Sol-Gel Methods and Their Application in Catalysis. *Catalysts*, 8(5), Article 5. <https://doi.org/10.3390/catal8050212>
- Wiley, B. (2022). *ALSEAL 5KGT VALIDATION: HEXAVALENT-CHROMIUM-FREE HEAT AND CORROSION RESISTANT (ALUMINUM) PAINT (LF IR45150-2) LYDCP4* (21ME-44145, Report ID 44145). Rolls Royce. [Available upon request from Rolls Royce].

Further Reading

- Dimitriev, Y., Ivanova, Y., & Iordanova, R. (2008). *HISTORY OF SOL-GEL SCIENCE AND TECHNOLOGY (REVIEW)*.
- Sakka, S. (2022). Birth of the sol–gel method: Early history. *Journal of Sol-Gel Science and Technology*, 102(3), 478–481. <https://doi.org/10.1007/s10971-021-05640-9>

Available Upon Request: More detailed microscopy images are available on request, but compositions will be removed or censored to protect the rights of Luna Labs.

Appendix

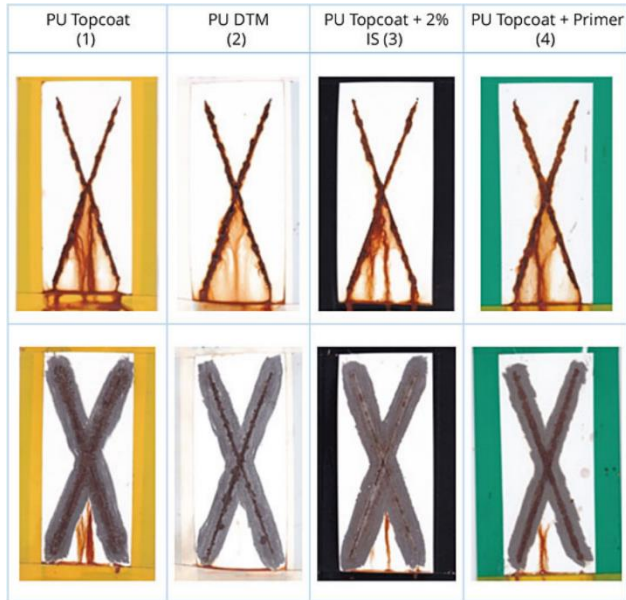


Figure A1. Typical appearance for ASTM 1654.

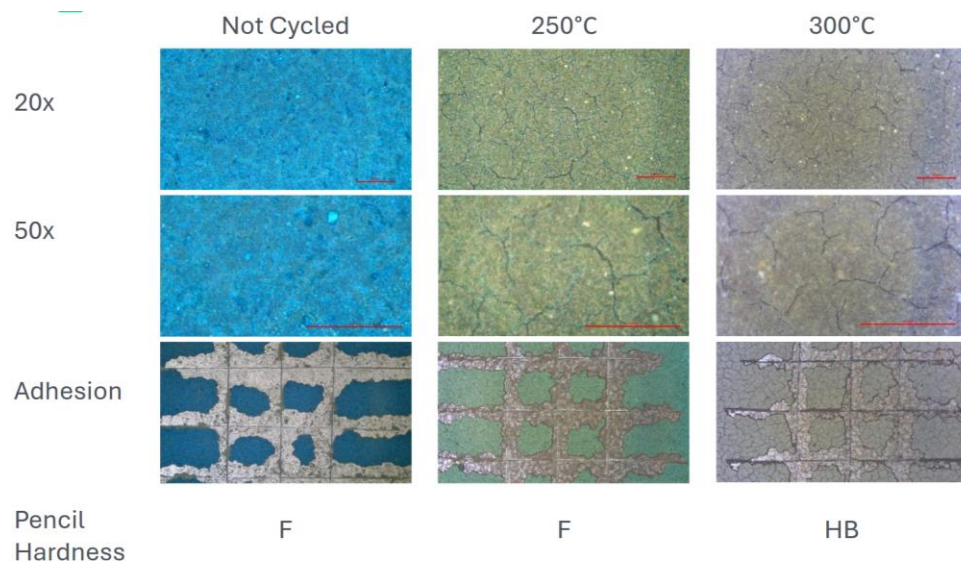


Figure A1. ZC+HTB1 thermal screening and adhesion.

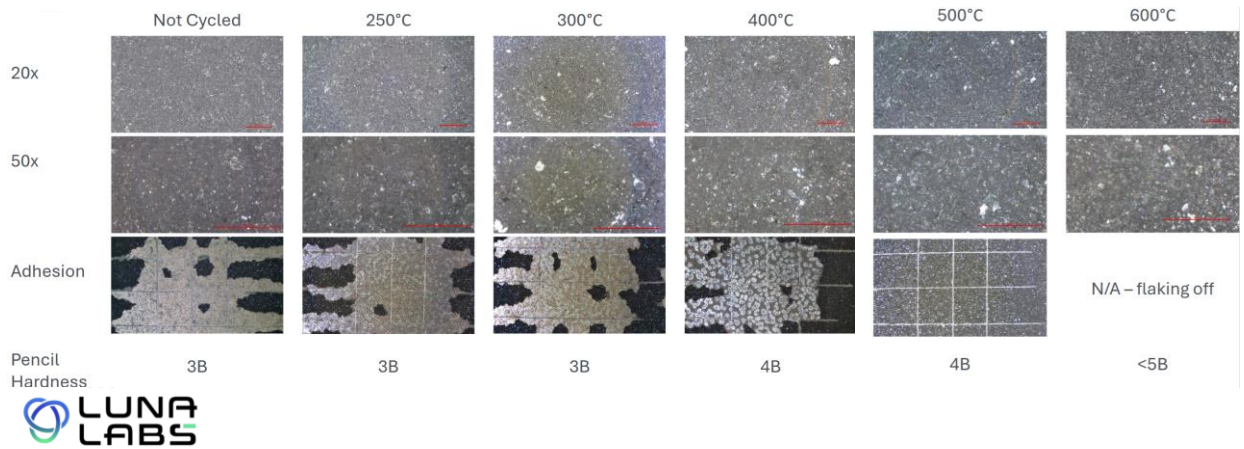


Figure A2. ZC+HTB2 thermal screening and adhesion. Note: microcracking evident past 300°C°.

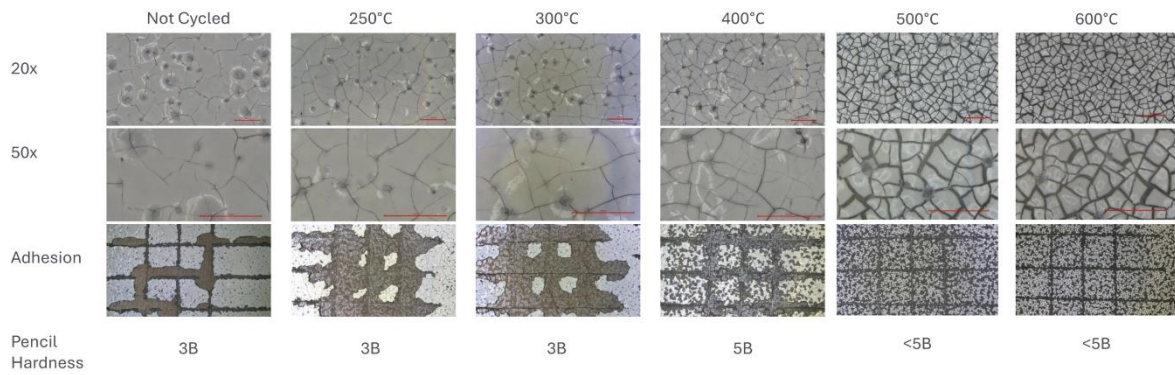


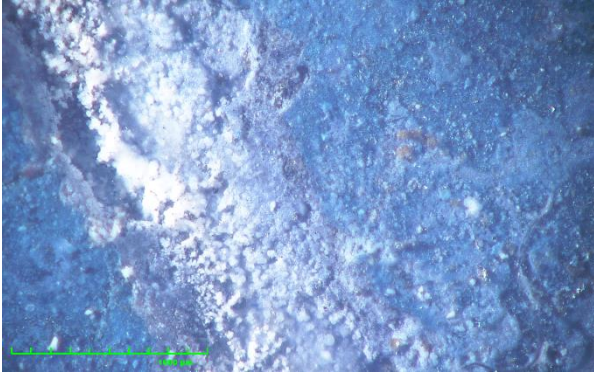
Figure A3. ZC+HTB4 thermal screening and adhesion.



50x



100x



100x (scribe)

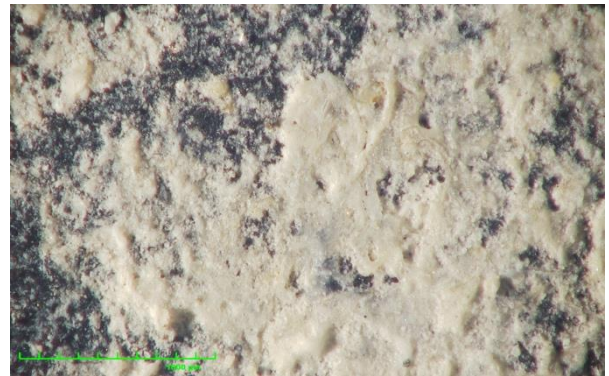


150x (scribe)

Figure A4. Comprehensive light micrograph summary for ZC+HTB1



50x



100x



100x

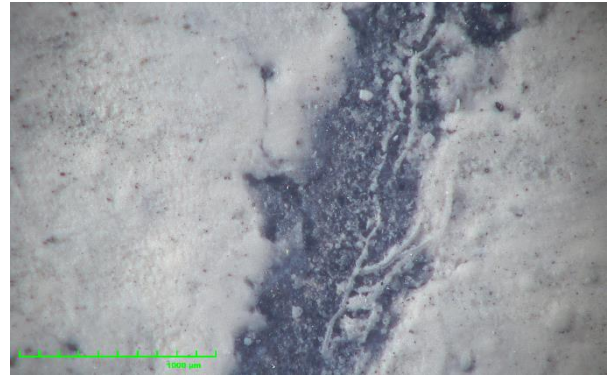


100x (scribe)

Figure A5. Comprehensive light micrograph summary for ZC+HTB2



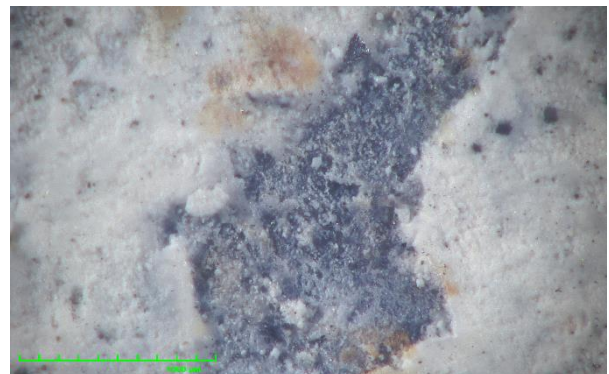
50x



100x (scribe)

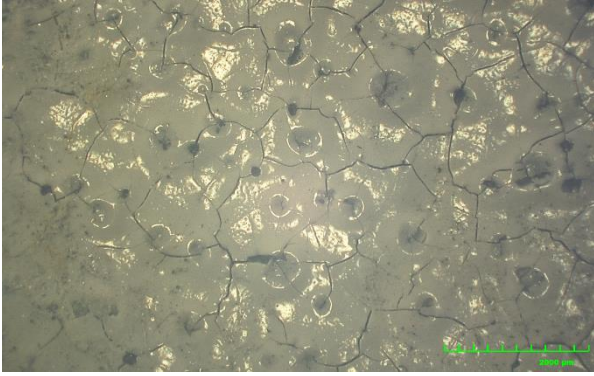


100x (unscribed)



100x (scribe)

Figure A6. Comprehensive light micrograph summary for ZC+HTB3



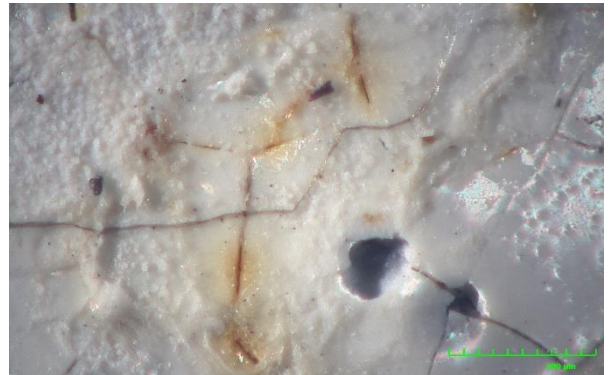
35x



100x



35x (scribe)



150x

Figure A7. Comprehensive light micrograph summary for ZC+HTB4



Figure A8. Delaminated HTB3 and ZC coating from scribed coupon.